Korean J. Chem. Eng., **28**(2),583-590 (2011)
DOI: 10.1007/s11814-010-0399-9

Adsorption dynamics and effects of carbon to zeolite ratio of layered beds for multicomponent gas adsorption

Seong-Cheol Jang*,, Se-Il Yang*, Seong-Geun Oh**, and Dae-Ki Choi*,†**

*Fuel Cell Center, Korea Institute of Science & Technology, 39-1 Hawolgok-dong, Seongbuk-gu, Seoul 136-791, Korea
**Major in Chemical Engineering, Hanyang University, 17 Haengdang-dong, Seongdong-gu, Seoul 133-791, Korea
(*Received 15 June 2010 • accepted 3 August 2010*)

Abstract−To optimize the performance of an adsorption bed, layered beds of activated carbon and zeolite 5A are used for multicomponent gas separation (H_2: 72.2%, CO_2: 21.6%, CO: 2.03%, CH_4: 4.17%). The adsorption dynamic characteristics were studied experimentally and theoretically using layered beds of activated carbon and zeolite 5A at 8 atm adsorption pressure and 16.67 L/min feed rate. Non-isothermal and non-adiabatic models, based on a linear driving force model and Dual-Site Langmuir adsorption isotherm model, were used. As the carbon ratio increased, the average velocity of CH_4 wavefront became slow, and wavefronts of CO and CO_2 propagated quickly on average.

Key words: Adsorption Dynamic, Layered Bed, Carbon to Zeolite Ratio, Hydrogen, Dual-Site Langmuir

INTRODUCTION

Hydrogen, regarded as an ecologically clean and renewable energy source, is increasingly in demand in various fields, including fuel cells, semiconductor processing, and the petrochemical industry. When steam reforming technology is applied to produce hydrogen, it is very important to remove other impurities (mainly CO, CO_2 and CH_4). Pressure swing adsorption (PSA), which is generally considered to be low in energy consumption and very precise in H_2 separation (99.99%) with the aid of pore size and surface characteristics of adsorbent [1,2], has been extensively used to obtain the desired purity of H_2 product.

Single-adsorbent H_2 PSA for binary or ternary mixtures with only single or two major impurities has been employed in previous works [3-5]. However, to obtain a high purity product from a multicomponent feed, commercialized H_2 PSA processes use more than one adsorbent simultaneously, because different adsorbents show different selectivity depending on the adsorbate. Therefore, an important characteristic of the H_2 PSA process is that many different adsorbents are used in multiple layered beds. In previous works, a layered bed was applied to a PSA process for improvement in efficiency and showed that the yield and productivity of the PSA process using double-layered beds was strongly dependent on the relative layer lengths [6-8]. Also, the adsorption dynamics in the bed and its optimal design were studied from the experiment and simulation at high pressure, above 15 atm, in the layered bed for H_2 mixture separation [9,10].

A basic study on the adsorption dynamics in a layered bed is very important because the adsorption step plays a key role in optimizing the performance of a cyclic process using layered beds. In this study, by using a layered bed packed with activated carbon and zeolite 5A, the adsorption dynamics were investigated experimentally and theoretically at low pressure (8 atm). Because the separation was strongly dependent on the ratio of the two layers, the effect of the carbon-to-zeolite ratio on the breakthrough was also investigated. The experimental results were analyzed with a non-isothermal and non-adiabatic model.

†To whom correspondence should be addressed.
E-mail: dkchoi@kist.re.kr

THEORY

In this study, an axially dispersed plug flow model was adopted and the linear driving force (LDF) approximation was used. Also, a complete non-isothermal and non-adiabatic dynamic model was adopted with the following assumptions [11-13]:

(1) The gas phase behaves as an ideal gas mixture.

(2) The flow pattern in the bed can be described by the axial dispersion plug flow model.

(3) The solid and gas phase reach thermal equilibrium instantaneously.

(4) Radial concentration and temperature gradients on the adsorption bed are negligible.

(5) The mass transfer rate is represented by a linear driving force expression.

(6) The multicomponent adsorption equilibrium is represented by the dual-site Langmuir.

Using the flow pattern described by the axial dispersion plug flow, the material balance for the bulk phase in the adsorption column is given by

$$-D_L\frac{\partial^2 C_i}{\partial z^2}+\frac{\partial uC_i}{\partial z}+\frac{\partial C_i}{\partial t}+\frac{1-\varepsilon}{\varepsilon}\rho_P\frac{\partial \bar{q}}{\partial t}=0 \tag{1}$$

And overall mass balance can be written as:

$$-D_L\frac{\partial^2 C}{\partial z^2}+\frac{\partial uC}{\partial z}+\frac{\partial C}{\partial t}+\frac{1-\varepsilon}{\varepsilon}\rho_P\sum_{i=0}^{n}\frac{\partial \bar{q}}{\partial t}=0 \tag{2}$$

where D_L is the axial dispersion coefficient. It can be calculated by the Wakao Eq. [14]:

$$\frac{D_L}{2uR_P}=\frac{20}{ReSc}+0.5 \tag{3}$$

In this model, the effects of all mechanisms which contribute to axial mixing are lumped together into a single effective axial dispersion coefficient, and it is possible to neglect axial dispersion and assume the ideal plug flow when the feed flow rate is high. However, mass transfer resistance at the external film and/or within the adsorbent particle is prominent at a low feed rate, the weight of the axial dispersion term is increased, making this term important.

If the ideal gas law applies to these equations, Eq. (1) and Eq. (2) can be transformed into

$$-D_L\frac{\partial^2 y_i}{\partial z^2}+u\frac{\partial y_i}{\partial z}+\frac{\partial y_i}{\partial t}+\frac{RT}{P}\frac{1-\varepsilon}{\varepsilon}\rho_P\left(\frac{\partial \bar{q}_i}{\partial t}-y\sum_{j=i}^{n}\frac{\partial \bar{q}_i}{\partial t}\right)=0 \tag{4}$$

And the overall mass balance can be represented as follows:

$$-D_L\frac{\partial^2 P}{\partial z^2}+P\frac{\partial u}{\partial z}+\frac{\partial P}{\partial t}-PT\left(-D_L\frac{\partial^2(1/T)}{\partial z^2}+u\frac{\partial(1/T)}{\partial z}+\frac{\partial(1/T)}{\partial t}\right)$$
$$+\frac{1-\varepsilon}{\varepsilon}\rho_P RT\sum_{j=i}^{n}\frac{\partial \bar{q}_i}{\partial t}=0 \tag{5}$$

Assuming thermal equilibrium between fluid and particles, the energy balance for the gas and solid phase is given by:

$$-K_L\frac{\partial^2 T}{\partial z^2}+\varepsilon\rho_g C_{pg}u\frac{\partial T}{\partial z}+(\varepsilon_t\rho_g C_{pg}+\rho_g C_{ps})\frac{\partial T}{\partial t}$$
$$-\rho_B\sum_{i=0}^{n}Q_i\frac{\partial \bar{q}_i}{\partial t}+\frac{2h_i}{R_{B_i}}(T-T_W)=0 \tag{6}$$

where, ε_t is the total void fraction and ρ_B is bulk density. K_L is the effective axial thermal conductivity used, taking into account the effective conduction in the axial direction. For the energy equation, the effective axial thermal conductivity, K_L, was estimated by using the empirical correlation given by Kunii and Smith and Yagi et al. as follows [15,16]:

$$\frac{K_L}{k_g}=\frac{K_{L_0}}{k_g}+\delta PrRe \tag{7}$$

$$\frac{K_{L_0}}{k_g}=\varepsilon+\frac{1-\varepsilon}{\varphi+\frac{2}{3}\frac{k_g}{k_s}} \tag{8}$$

$$\varphi=\varphi_2+(\varphi_1-\varphi_2)\left(\frac{\varepsilon-0.216}{0.216}\right)\quad \text{for } 0.260\le\varepsilon\le 0.476 \tag{9}$$

For all the simulations conducted in this study, the following parameter values were adopted:

$$(\delta, \varphi_1, \varphi_2)=(0.75, 0.2, 0.1) \tag{10}$$

In Eq. (6), the last term, heat transfer to the wall, can be neglected if the heat capacity of wall is not large compared to that of particles. However, since the diameter of the adsorption bed in the present study was rather small, heat loss through the wall and heat accumulation in the wall could not be neglected. Therefore, an energy balance for the wall of the adsorption bed was constructed with the assumption of neglecting axial conduction in the wall:

$$\rho_W C_{PW}A_W\frac{\partial T_W}{\partial t}=2\pi R_{B_i}h_i(T-T_W)-2\pi R_{B_0}h_0(T-T_{atm}) \tag{11}$$

$$A_W=\pi(R_{B_0}^2-R_{B_i}^2) \tag{12}$$

The Danckwerts boundary conditions are applicable for the component balance. The boundary condition and the initial conditions are in the following forms:

Boundary condition at z=0 and z=L for fluid flow

$$-D_L\left(\frac{\partial y_i}{\partial z}\right)\Big|_{z=0}=u(y_i|_{z=0^-}-y_i|_{z=0^+});\ \left(\frac{\partial y_i}{\partial z}\right)\Big|_{z=L}=0 \tag{13}$$

$$-K_L\left(\frac{\partial T}{\partial z}\right)\Big|_{z=0}=\rho_g C_{pg}u(T|_{z=0^-}-T|_{z=0^+});\ \left(\frac{\partial T}{\partial z}\right)\Big|_{z=L}=0 \tag{14}$$

where $y_i|_{z=0}$ means feed composition for component i

Velocity boundary condition at z=0 and z=L:

$$u|_{z=0}=u_0;\ \left(\frac{\partial u}{\partial z}\right)\Big|_{z=L}=0 \tag{15}$$

Initial condition for saturated bed:

$$C_i(z,0)=C_0;\ \bar{q}_i(z,0)=q_i^* \tag{16}$$

$$T(z,0)=T_{atm} \tag{17}$$

Pore diffusion, surface diffusion, and solid diffusion are the representative diffusion mechanisms that are considered in this field. Also, intraparticle convection is considered for a large pore adsorbent, giving intermediate behavior of the diffusion model and the equilibrium model. However, it is very difficult to consider all the kinetic mechanisms for the purpose of representing sorption rates within adsorbent particles. The sorption rate into an adsorbent pellet is described by the following LDF model [17], which involves many possible mass transfer phenomena within a porous medium and external mass transfer into a single lumped mass transfer parameter, k

$$\frac{\partial \bar{q}_i}{\partial t}=k_i(q_i^*-\bar{q}_i) \tag{18}$$

Where q* is the adsorbed-phase concentration in equilibrium with the local bulk phase concentration, and k is an LDF mass transfer coefficient, which can be estimated by the following equation:

$$\frac{1}{Kk}=\frac{R_P}{3k_f}+\frac{R_P^2}{15\varepsilon_P D_P}+\frac{r_c^2}{15KD_c} \tag{19}$$

Eq. (19) is only applicable when the equilibrium is linear or at least not severely nonlinear and justified by an analysis of the moments of the dynamic response. Although the sorption model is rather simple, this rate model has been used extensively, regardless of the adsorbate-adsorbent system in an equilibrium-controlled separation. This is because the adsorption process models using this sorption model predict experimental data with satisfactory accuracy [18].

The equilibrium isotherms are assumed to be described by dual-site Langmuir model [19-21].

$$q_i=\frac{q_{m,1}B_{i1}Py_i}{1+\sum_k(B_{k1}Py_k)}+\frac{q_{m,2}B_{i2}Py_i}{1+\sum_k(B_{k2}Py_k)} \tag{20}$$

$q_{m1}=k_1$, $B_1=k_2\exp(k_3/T)$

$q_{m2}=k_4$, $B_2=k_5\exp(k_6/T)$

The governing partial differential equations were solved in space and the resulting ordinary differential equations are solved using Aspen ADSIM from Aspen Technology Inc.

Table 1. Physical properties of adsorbents and bed

Adsorbents			
		Activated carbon	Zeolite 5A
Average pellet size	(mm)	1.15	1.57
Pellet density	(g/cm^3)	0.85	1.16
Bulk density	(g/cm^3)	0.498	0.734
Heat capacity	(cal/g·K)	0.25	0.21
Bed			
Length	(cm)	170	
Inside diameter	(cm)	3.84	
Outside diameter	(cm)	0.51	
Heat capacity of column	(cal/g·K)	0.12	
Density of column	(g/cm^3)	7.83	
Internal heat transfer coefficient	(kJ/s·m^3·K)	0.0385	
External heat transfer coefficient	(kJ/s·m^3·K)	0.0142	
Bulk density	(g/cm^3)	0.532	0.744
External void fraction	(-)	0.433	0.357

EXPERIMENTAL

The adsorbents in this experiment were activated carbon (Calgon Co.) and zeolite 5A (W. R. Grace Co.). The physical properties tabulated in Table 1 are the manufacturer's reported values. Before each experimental run, the adsorbents were regenerated for more than 24 h at 473 K. The adsorbate used is a premixed gas mixture (H_2: 72.2%, CO_2: 21.6%, CO: 2.03%, CH_4: 4.17%).

A schematic diagram of the breakthrough apparatus is presented in Fig. 1, and characteristics of adsorption bed are presented in Table 1. The adsorption bed was made of stainless steel 170 cm in length and 3.84 cm inside diameter and 0.51 cm wall thickness. The section in both ends of the column was filled with glass wool and metal screen to prevent the carryover of adsorbent particles. Seven K-type thermocouples were installed at the positions of 10, 35, 60, 85, 110, 135, and 160 cm from the top of the packed section, at the center, and at half the bed radius in order to track the thermal wavefront. A pressure transducer (Sensys Tech.) was installed at the top of the bed in order to measure the pressure variation. The gas flow to the bed was controlled by a mass flow controller (Bronkhorst High-Tech) which was precalibrated by a wet gas meter (Shinagawa). An electrical back pressure regulator (Bronkhorst High-Tec) was installed to maintain a constant adsorption pressure in the bed. The sampling port was placed downstream of the mass flow meter (Bronkhorst High-Tec), so that the product flow rate could be measured without any loss resulting from sampling. The product concentrations were monitored continuously and automatically with a mass spectrometer (Omnistar 300). The control of the solenoid valve switching and the data acquisition of measuring variables were done by a PLC (National Instruments) linked to a personal computer whose monitor provided an on-line display of the dynamic changes in all measured values.

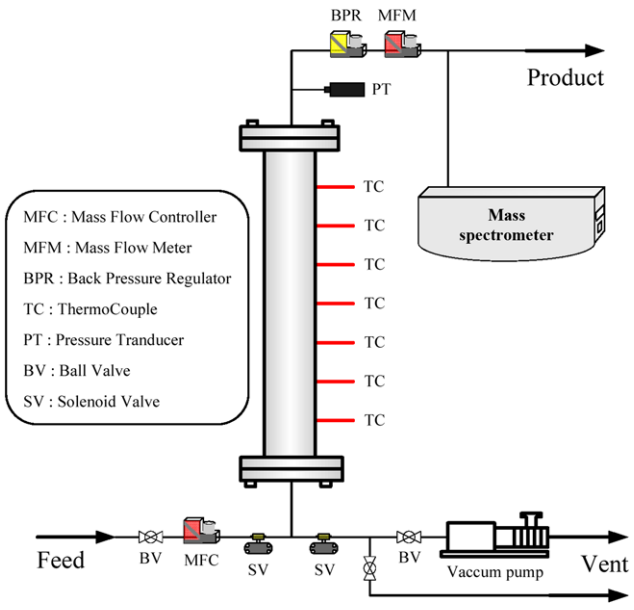

Fig. 1. A schematic diagram of the breakthrough apparatus.

Prior to the experiment, adsorbents were packed in the bed after regeneration in a drying vacuum oven at 473.15 K for more than 24 h to remove impurities. The packed bed was evacuated by a high vacuum pump to remove traces of impurities, and was then purged with hydrogen. The required flow and the corresponding system pressure were adjusted with hydrogen.

In this study, breakthrough curves were obtained with the single adsorbent bed, which have a zeolite 5A bed and the activated carbon bed, and two kinds of layered beds, which have 0.5 and 0.7 carbon ratios, respectively, at 8 atm adsorption pressure and 16.67 L/min feed rate. A carbon ratio defined the ratio of an activated carbon layer length to a bed length [10,22].

RESULTS AND DISCUSSION

1. Adsorption Equilibrium

Before the breakthrough experiment, adsorption equilibriums were measured. The adsorption isotherms for all pure gas were obtained from a volumetric method. Isotherm curves were measured at three temperatures (293.15, 303.15, and 313.15 K) for both zeolite 5A and activated carbon. Fig. 2 shows the equilibrium isotherms on zeolite 5A and activated carbon at 293.15 K. CO_2 is the most strongly adsorbed component for both adsorbents, while H_2 is the weakest. Zeolite 5A is saturated with CO_2 at low pressure, indicating that CO_2 is very difficult to desorb. The amount of CH_4 adsorbed on the activated carbon was larger than that on zeolite 5A, but the reverse was true for the CO. Park et al. (1998) reported adsorption equilibrium for these four gases on zeolite 5A and activated carbon [9]. Although the adsorbents were from different manufacturers, the adsorption equilibriums were nearly identical.

In this study, the dual-site Langmuir (DSL) isotherm, bimodal two-site discrete distribution of the Langmuir, was employed for all pure gas. This isotherm is popular for bulk gas separation [20]. The isotherm parameters on the activated carbon and zeolite 5A were obtained by matching the experimental data with the DSL isotherm, respectively.

The isosteric heat of adsorption can be calculated by the Clausius-Clapeyron equation of adsorption. The pure-gas isosteric heat

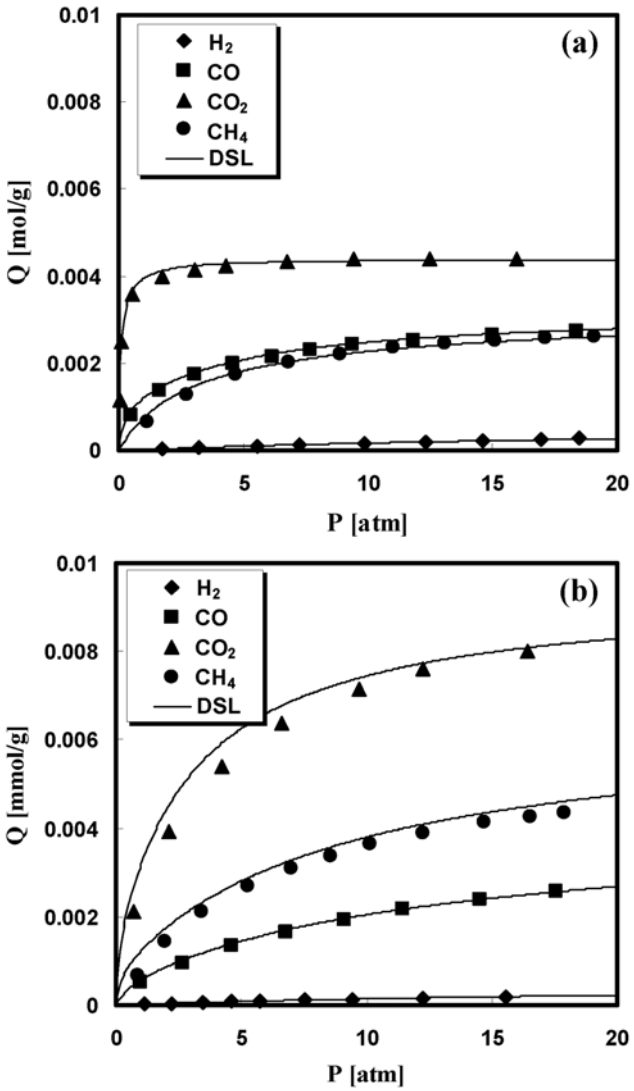

Fig. 2. Adsorption isotherm of CH_4, CO, CO_2, and H_2 at 293.15 K. (a) zeolite 5A and (b) activated carbon.

of adsorption at 293.15 K was calculated by the DSL model. The isotherm parameters and the values of heats of adsorption are given in Table 2.

2. Single Adsorbent Bed

For the zeolite 5A bed in Fig. 3, CH_4 was the first breakthrough component. The breakthrough of CO appeared later and, finally,

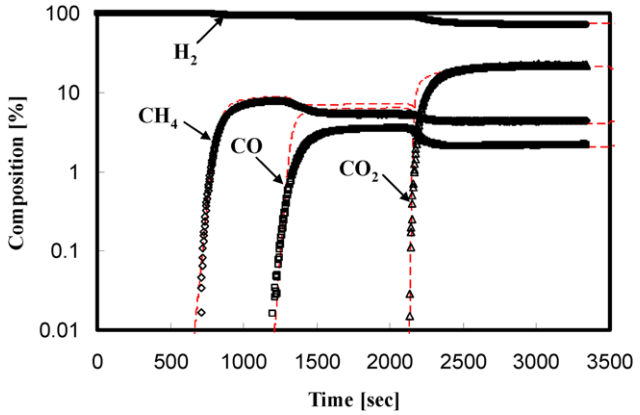

Fig. 3. Breakthrough curves in the zeolite 5A bed under 16.67 L/min feed flow rate and 8 atm adsorption pressure. Symbols: experiment results; ----: simulation results.

that of the CO_2 occurred in the adsorption bed at about 2,100 sec. The first roll-up of the CH_4 breakthrough curve is due to the CO. After, the CO also shows the roll-up phenomenon, which is due to competitive adsorption with the more strongly adsorbed component, CO_2. The well-known roll-up phenomenon results from the fact that weakly adsorbed components lose their adsorption sites due to the competitive adsorption of the stronger adsorbed components that follow the preceding wavefronts of weakly adsorbed components. The desorbed adsorbates join the bulk stream and increase the concentration more than the feed concentration [8,23]. These breakthrough curve phenomena were reflected in the temperature profile. Fig. 4 shows the temperature histories of four bed locations at 10, 60, 110, and 160 cm. As shown in the figure, the temperature variation was large, about 110 K, on the zeolite 5A bed. This implies that the energy balance equations must be included in modeling and the temperature curves demonstrate the importance of the heat of adsorption in the gas adsorption process [11]. Because the concentration wavefronts of CO, CO_2, and CH_4 at the feed end were close, one temperature excursion is shown at a length of 10 cm. However, the three wave velocities of CO, CO_2, and CH_4 became significantly different. Therefore, a stepwise temperature excursion occurred at lengths of 60, 110 and 160 cm. Moreover, at a length of 60 cm, the first excursion of the temperature profile by the CH_4 concentration decreased slightly because of heat transfer and desorption of CH_4 by the adsorption of CO. Also, as the mixture gases reached the end of the bed, the interval of the temperature excur-

Table 2. Dual-Site Langmuir parameters and heat of adsorption

		k_1 [mmol/g]	k_2 [1/atm]	k_3 [K]	k_4 [mmol/g]	k_5 [1/atm]	k_6 [K]	Q_i [cal/mol]
Activated carbon	H_2	2.40E-5	9.0E-4	1700	4.80E-4	6.0E-5	1915	−1800
	CO	3.65E-3	8.7E-5	2003	4.37E-4	2.0E-3	2050	−4000
	CH_4	5.80E-3	1.0E-4	2060	7.40E-4	3.5E-3	2200	−5600
	CO_2	8.00E-3	8.0E-6	3100	1.40E-3	9.6E-7	4750	−5900
Zeolite 5A	H_2	7.8E-4	9.0E-5	1647	7.0E-6	1.2E-5	3000	−1500
	CO	2.3E-3	9.7E-5	2920	9.5E-4	7.9E-5	3280	−7000
	CH_4	2.6E-3	2.1E-4	2200	7.5E-4	3.0E-9	4800	−4600
	CO_2	3.0E-3	1.1E-3	2508	1.4E-3	1.0E-2	3300	−8500

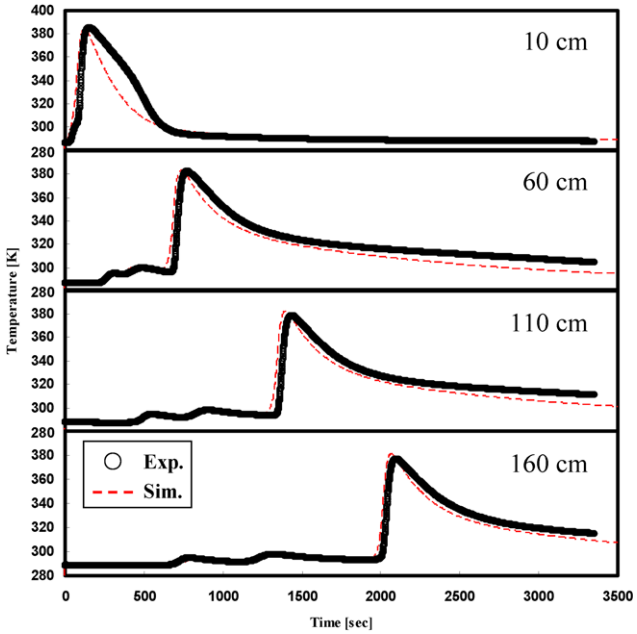

Fig. 4. Temperature histories in the zeolite 5A bed under 16.67 L/min feed flow rate and 8 atm adsorption pressure. Symbols: experiment results; ----: simulation results.

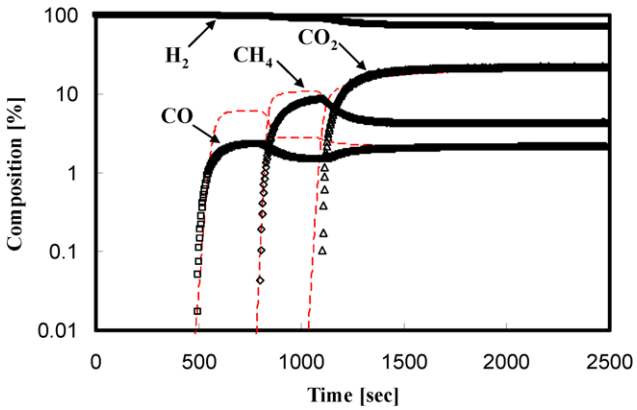

Fig. 5. Breakthrough curves in the activated carbon bed under 16.67 L/min feed flow rate and 8 atm adsorption pressure. Symbols: experiment results; ----: simulation results.

sion became wider because the adsorption capacities of CO, CO_2 and CH_4 are different.

The result of the breakthrough experiment by using the activated carbon bed is shown in Fig. 5. Unlike the zeolite 5A bed, CO was the first breakthrough component because of the increased adsorption capacity for CH_4 in the activated carbon bed: the breakthrough time of CH_4 was elongated more than that in the zeolite 5A bed. After, the CH_4 breakthrough and shows roll-up phenomenon because of competitive adsorption with the more strongly adsorbed component, CO_2. Fig. 6 shows the temperature histories of four bed locations at 10, 60, 135, and 160 cm. Compared to those shown in Fig. 3, the peak of the temperature excursion was small, about 40 K, on the activated carbon bed. This is the reason that the heat of adsorption of CO_2 on activated carbon is lower than on zeolite 5A. At a length of 60 cm, the first peak of the temperature excursion

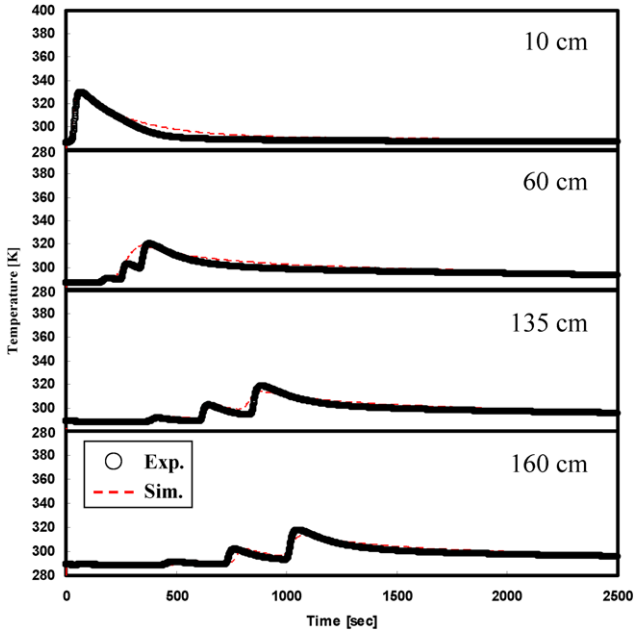

Fig. 6. Temperature histories in the activated carbon bed under 16.67 L/min feed flow rate and 8 atm adsorption pressure. Symbols: experiment results; ----: simulation results.

occurred by the CO and then the second peak of the temperature excursion occurred by the CH_4. The last peak of the temperature excursion occurred by the CO_2. Also, like the zeolite 5A bed, as the mixture gases are reached at the end of the bed, the interval of the temperature excursion become wider.

3. Layered Bed

In the single adsorbent bed, we confirmed that the activated carbon strongly adsorbed CH_4, and a zeolite 5A strongly adsorbed CO. Therefore, in order to maximize the utilization of adsorbents, a layered bed containing the activated carbon and zeolite 5A must be used for multicomponent separation by PSA process. Typically, the first layer adsorbs a strongly adsorptive component, and the second layer removes light components [2]. Yang and Lee determined that there might be an optimum carbon ratio for layered bed H_2 PSA through breakthrough experiments using a layered bed with a ratio of 0.65 [10]. Chlendi et al. showed that the yield and the productivity of the PSA using double layered beds were strongly dependent on the relative layer lengths [8]. The separation was again strongly dependent on the ratio of the two layers. Therefore, for a given operating condition the optimal design of the length of each layer is important through adsorption dynamic.

Fig. 7 shows the breakthrough curves of a layered bed that has a carbon ratio of 0.5 at 8 atm adsorption pressure and 16.67 L/min feed rate. CH_4 was the first break through component, followed by CO. The second breakthrough of CO appeared, and finally, that of CO_2 occurred in the adsorption bed. The breakthrough curves for a layered bed show an intermediate behavior of the breakthrough curves shown in Figs. 3 and 5.

Fig. 8 shows the breakthrough curves of a layered bed that has a carbon ratio of 0.7 at the same feed rate and pressure as the preceding breakthrough experiment. Compared to that shown in Fig. 7, the breakthrough of CH_4 and CO occurred almost simultaneously.

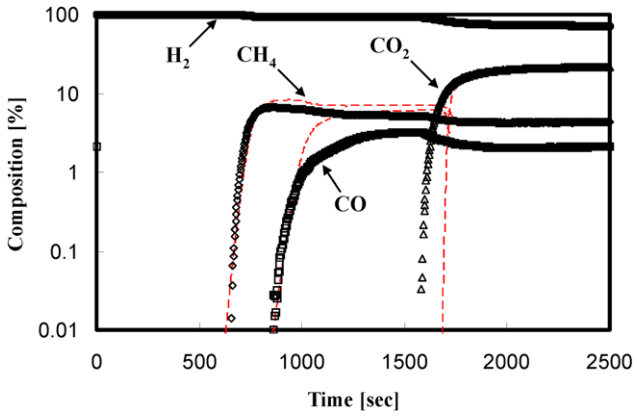

Fig. 7. Breakthrough curves in a layered bed (carbon ratio=0.5) under 16.67 L/min feed flow rate and 8 atm adsorption pressure. Symbols: experiment results; ----: simulation results.

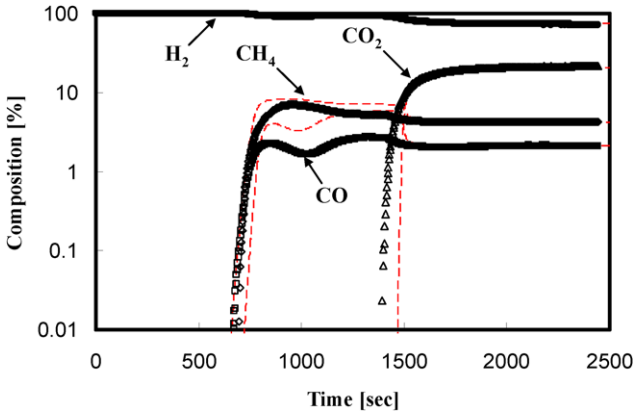

Fig. 8. Breakthrough curves in a layered bed (carbon ratio=0.7) under 16.67 L/min feed flow rate and 8 atm adsorption pressure. Symbols: experiment results; ----: simulation results.

Also, the double roll-ups of the CO breakthrough curve occurred because of the layered beds. Compared to the pure activated carbon bed, the breakthrough times of CO and CO_2 except CH_4 were longer. As carbon ratio decreased, the longer breakthrough of CO and CO_2 in the layered bed was attributed to the smaller amount adsorbed on activated carbon than on zeolite 5A. The earlier breakthrough of CH_4 in the layered bed was attributed to the smaller amount adsorbed on zeolite 5A than on activated carbon.

The temperature histories are shown in Figs. 9 and 10. In 0.5 of carbon ratio, the temperature at 110 cm from the entrance where the bed was packed with zeolite 5A had two separate temperature peaks. These, again, were combined thermal waves. In 0.7 of carbon ratio, temperature peaks at 160 cm were combined thermal waves. Because the concentration wavefront of CH_4 caught up with that of CO in the zeolite layer, the two peaks of the temperature peaks became combined. The first temperature peak was associated with the CO and CH_4 wave, while the second temperature peak was CO_2 wave.

To gain a clearer insight into the adsorption dynamics of layered beds, concentration profiles in the gas phase after 300, 500, 600, and 700 sec from the beginning of step input of feed are presented.

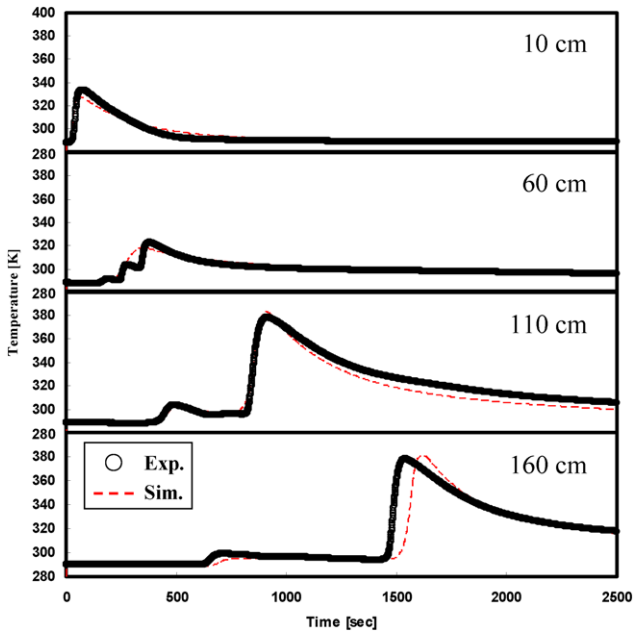

Fig. 9. Temperature histories in a layered bed (carbon ratio=0.5) under 16.67 L/min feed flow rate and 8 atm adsorption pressure. Symbols: experiment results; ----: simulation results.

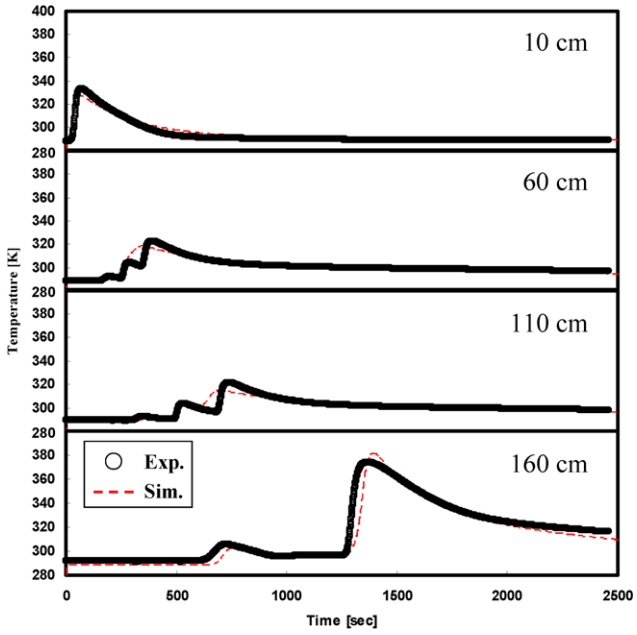

Fig. 10. Temperature histories in a layered bed (carbon ratio=0.7) under 16.67 L/min feed flow rate and 8 atm adsorption pressure. Symbols: experiment results; ----: simulation results.

Fig. 11 shows the results of 0.5 of carbon ratio for concentration profiles. At 300 sec, the fastest wavefront is CO, followed by the CH_4 front, and finally the CO_2 front. As the adsorption time increased from 300 to 500 sec, the CH_4 wavefront caught up with the CO wavefront in the zeolite 5A layer, because the adsorption capacity of CH_4 on the zeolite 5A is larger than that of CO. Therefore, as shown in Fig. 7, after 700 sec, CH_4 was the first breakthrough component. Also, the CO_2 wavefront is narrower in the zeolite 5A layer than in

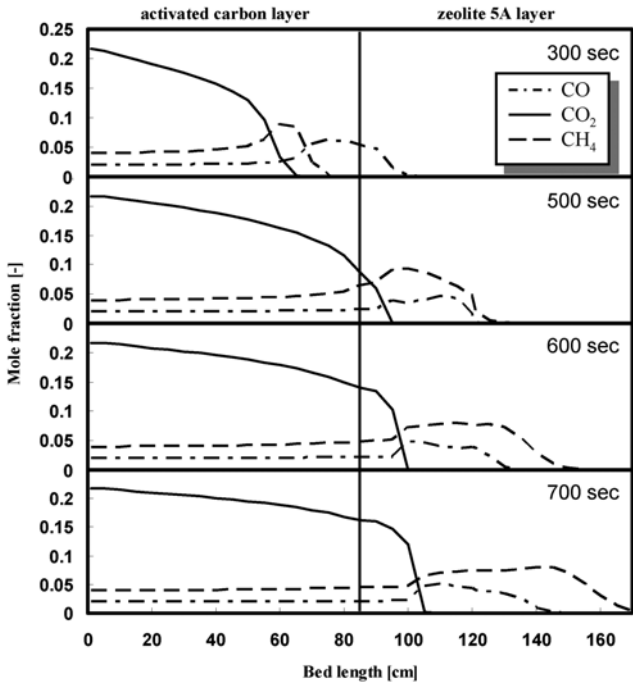

Fig. 11. Profiles of concentration in a layered bed (carbon ratio= 0.5) under 16.67 L/min feed flow rate and 8 atm adsorption pressure. Symbols: experiment results; ----: simulation results.

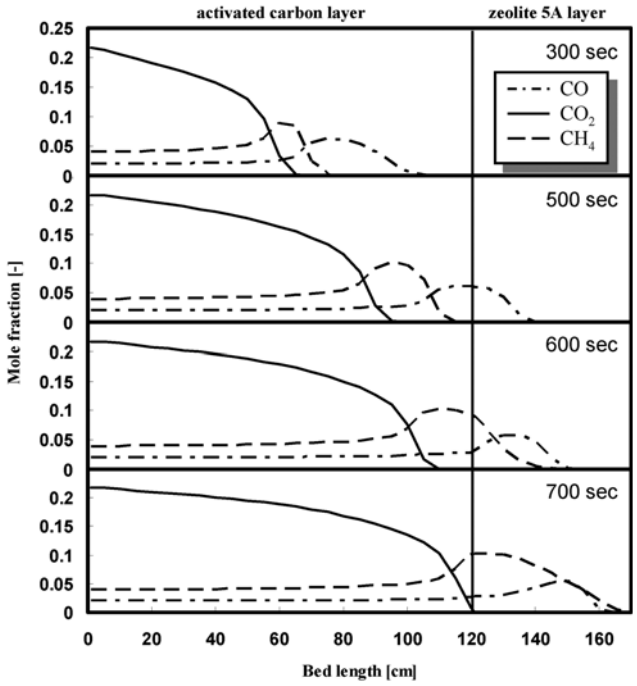

Fig. 12. Profiles of concentration in a layered bed (carbon ratio= 0.7) under 16.67 L/min feed flow rate and 8 atm adsorption pressure. Symbols: experiment results; ----: simulation results.

the activated carbon layer, because zeolite 5A is saturated with CO_2 at low pressure. On the other hand, as shown in Fig. 12, when the carbon ratio is 0.7, the CH_4 wavefront caught up with the CO wavefront at about 700 sec, the breakthrough times of CH_4 and CO were then similar. At the same time, the CO_2 had not broken through into the zeolite 5A. Desorption of CO_2 is very difficult due to the steepness of the isotherm at low pressure. Thus, when the design of a layered bed is determined, CO_2 must not break through into the zeolite 5A.

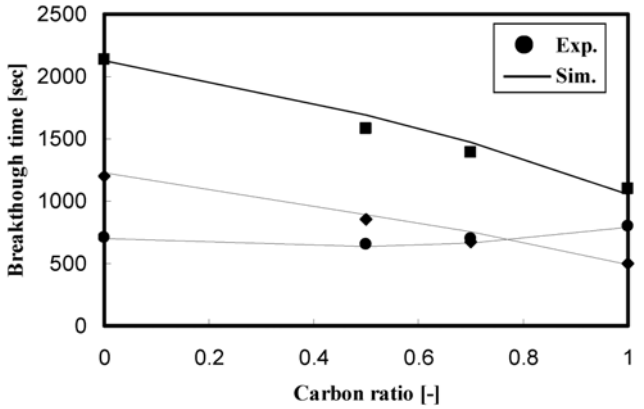

Fig. 13. Effect of carbon ratio on breakthrough time under 16.67 L/min feed flow rate and 8 atm adsorption pressure (●: CH_4, ◆: CO, ■: CO_2).

4. Effect of Carbon Ratio on Breakthrough Time

Fig. 13 shows the variations of breakthrough times with the carbon ratio at 8 atm adsorption pressure and 16.67 L/min feed rate. As the carbon ratio increased, the breakthrough time of CO and CO_2 except CH_4 is shorter and the breakthrough time of CO and CH_4 cross at about 0.7 carbon ratio. The impurities, CO and CH_4, were important for determining the optimum carbon ratio. While the zeolite 5A bed gave the best performance when CH_4 was not present in the feed, the carbon ratio should be increased until about 0.7 if CH_4 is present in the feed because the breakthrough of CO occurred if the carbon ratio was too large. When the carbon ratio was about 0.7, the breakthrough of CH_4 and CO occurred almost simultaneously and CO_2 was not broken through into zeolite 5A.

CONCLUSION

The adsorption dynamics of the single adsorbent bed and layered beds packed with activated carbon and zeolite 5A was studied through breakthrough experiments at 8 atm adsorption pressure and 16.67 L/min feed rate. All the essential characteristics of adsorption dynamics were well predicted by a non-isothermal and non-adiabatic model using the dual-site Langmuir isotherm.

The activated carbon strongly adsorbed CH_4, and a zeolite 5A strongly adsorbed CO because adsorbents show different selectivity depending on the adsorbate. In the single adsorbent bed, the activated carbon bed and the zeolite 5A bed showed the different results of breakthrough curves by different adsorption equilibrium. Also, a layered bed showed an intermediate like that of the zeolite 5A bed and the activated carbon bed.

The impurities, CH_4 and CO, were important for determining the optimum carbon ratio, while the zeolite 5A bed gave the best performance when CH_4 was not present in the feed. When the carbon ratio is smaller than 0.7, the breakthrough time of CH_4 is shorter

than that of CO. Also, when the carbon ratio is larger than 0.7, the breakthrough time of CO is shorter than CH_4. The breakthrough of CH_4 and CO occurred almost simultaneously, at about 0.7 carbon ratio and the CO_2 was not broken through into zeolite 5A.

NOMENCLATURE

A_w : cross sectional area [cm^2]
C : concentration of adsorbate [mol/g]
C_{pg} : gas heat capacity [cal/g/K]
C_{ps} : particle heat capacity [cal/g/K]
C_{pw} : column wall heat capacity [cal/g/K]
D_L : Knudsen diffusivity [cm^2/s]
h : heat transfer coefficient [$cal/cm^2 \cdot s \cdot K$]
k : linear driving force mass transfer coefficient [s^{-1}]
$k_{1\text{-}6}$: Dual-Site Langmuir isotherm model parameter
K_L : effective axial thermal conductivity [$cal/cm^2 \cdot s \cdot K$]
P : pressure [atm]
q : equilibrium mole adsorbed [mol/g]
q^* : equilibrium adsorbed phase concentration [mol/g]
Q : average isosteric heat of adsorption [cal/mol]
R : gas constant [cal/mol·K]
R_B : bed radius [cm]
t : time [s]
T : temperature [K]
T_{atm} : ambient temperature [K]
T_w : wall temperature [K]
u : interstitial velocity [cm/s]
V : volume [cm^3]
y : mole fraction in gas phase
z : axial position in a adsorption column [cm]

Greek Letters

ε : interparticle void fraction
ε_t : total void fraction
ρ_B : bulk density [cm^3/g]
ρ_g : gas density [cm^3/g]
ρ_p : particle density [cm^3/g]
ρ_w : column density [cm^3/g]

REFERENCES

1. D. M. Ruthven, *Principle of adsorption and adsorption processes*, John Wiley & Sons, New York (1984).
2. R. T. Yang, *Gas separation by adsorption processes*, Butterworths (1987).
3. S. J. Doong and R. T. Yang, *AIChE J.*, **32**, 397 (1986).
4. R. Kumar, *Ind. Eng. Chem. Res*., **33**, 1600 (1994).
5. J. Y. Yang, J. W. Chang and C. H. Lee, *Ind. Eng. Chem. Res.*, **36**, 2789 (1997).
6. D. D. Frey, *Sep. Sci. Technol*., **17**, 1485 (1983).
7. P. C. Wankat and D. Tondeur, *AIChE Symp. Ser.*, **81**, 74 (1985).
8. M. Chlendi, D. Tondeur and F. Rolland, *Gas. Sep. Purif.*, **9**, 125 (1995).
9. J. H. Park, J. N. Kim, S. H. Cho, J. D. Kim and R. T. Yang, *Chem. Eng. Sci.*, **53**, 3951 (1998).
10. J. Y. Yang and C. H. Lee, *AIChE J.*, **44**, 1325 (1998).
11. B. U. Choi, G. M. Nam, D. K. Choi, B. K. Lee, S. H. Kim and C. H. Lee, *Korean J. Chem. Eng.*, **21**, 821 (2004).
12. W. E. Waldron, Sicar, *Adsorption 6*, 179 (2000).
13. H. W. Ahn, J. Y. Yang and C. H. Lee, *Adsorption 7*, 339 (2001).
14. N. Wakao and T. Funazkri, *Chem. Eng. Sci.*, **33**, 1375 (1978).
15. D. Kunii and J. M. Smith, *AIChE J.*, **6**, 71 (1960).
16. S. Yagi, D. Kunii and N. Wakao, *AIChE J.*, **6**, 543 (1960).
17. D. M. Ruthven, S. Farooq and K. S. Knaebel, *Pressure swing adsorption*, VCH Publishers, New York (1994).
18. T. Panczyk and W. Rudzinski, *Korean J. Chem. Eng.*, **21**, 206 (2004).
19. P. M. Mathias, R. Kumar, J. D. Moyer, J. M. Schork, S. R. Srinivasan, S. R. Auvil and O. Talu, *Ind. Eng. Chem. Res.*, **35**, 2477 (1996).
20. L. T. Biegler and V. G. Jiang, *Sep. Purif. Res.*, **33**, 1 (2004).
21. E. S. Ahn, S. E. Jang, D. Y. Choi, S. H. Kim and D. K. Choi, *Korean Chem. Eng. Res.*, **44**, 460 (2006).
22. C. H. Lee, J. Y. Yang and H. W. Ahn, *AIChE J.*, **45**, 535 (1999).
23. C. C. Huang and J. R. Fair, *AIChE J.*, **34**, 1861 (1988).